Size-Dependent Optical Properties of VO_2 Nanoparticle Arrays

R. Lopez,* L. C. Feldman,† and R. F. Haglund, Jr.
Department of Physics and Astronomy, Vanderbilt University, Nashville, Tennessee 37235, USA
(Received 9 June 2004; published 20 October 2004)

The size effects on the optical properties of vanadium dioxide nanoparticles in ordered arrays have been studied. Contrary to previous VO_2 studies, we observe that the optical contrast between the semiconducting and metallic phases is dramatically enhanced in the visible region, presenting size-dependent optical resonances and size-dependent transition temperatures. The collective optical response as a function of temperature presents an enhanced scattering state during the evolving phase transition. The effects appear to arise because of the underlying VO_2 mesoscale optical properties, the heterogeneous nucleation behind the phase transition, and the incoherent coupling between the nanoparticles undergoing an order-disorder-order transition. Calculations that support these interpretations are presented.

DOI: 10.1103/PhysRevLett.93.177403 PACS numbers: 78.67.Bf, 36.40.Ei, 64.70.Nd

The study of photon-matter interactions at nanometer length scales has as its ultimate goal the optimization of the coupling between selected radiation modes and specific material excitations. Among the most exciting prospects are those that incorporate metal or semiconductor nanostructures into periodic arrays, with potential applications as photonic crystals [1], biochemical sensors [2], and near-field electromagnetic waveguides [3]. In periodic arrays of nanostructures, new properties arise from the combination of nanoscale material features and the periodicity of the arrays. These include the size-dependent and shape-dependent shift of optical resonances, and near-field or far-field coupling already observed in two-dimensional metal nanoparticle arrays [4–7].

In this Letter, we describe first observations of the collective optical response of vanadium dioxide nanoparticle (NP) arrays during a reversible semiconductor-to-metal phase transition (SMT). A previously unreported resonance in the visible region is found in the spectral signature of the SMT, and the resonance peak, apparently due to multipole effects, is blueshifted with decreasing NP size. Unlike the hysteretic response of VO_2 NPs with inhomogeneous size and spatial distributions, the hysteresis associated with the NP arrays shows a distinctive three-state behavior resulting from the differential scattering efficiency between the metal and semiconducting phases of VO_2. This unique optical response may be viewed as an order-disorder transition in the spectral response of the array, superimposed on the hysteretic response of individual NPs, and contains significant new insights about the stochastic nature of the mechanism that triggers the metal-insulator transition.

VO_2 exhibits a SMT at a critical temperature $T_c \sim 67\,^{\circ}\mathrm{C}$ that is a result of an atomic rearrangement. Above T_c, VO_2 has a tetragonal rutile structure and exhibits metallic properties. Below T_c, VO_2 is a narrow-gap semiconductor with a monoclinic unit cell [8]. The reversible VO_2 SMT displays a 10^4 jump in conductivity and large changes in the optical properties, especially in the infrared (IR) where VO_2 tends to some degree of transparency when a semiconductor and great opacity when a metal. Apart from the long and controversial history of mechanistic questions about this phase transition [9,10], VO_2 is a candidate material for a variety of technological applications that encompass, among others, ultrafast optical limiting since the SMT (both lattice and electronic structures) occurs in less than 500 fs [11].

VO_2 NP arrays were fabricated by a combination of ion beam lithography, pulsed laser deposition, and thermal oxidation. A solution of poly(methyl-methacrylate) (PMMA) (standard molecular weight of 950 kDa) in anisole (1.7% by weight) was spun onto a Si substrate and baked on a hot plate at 180 ° C for 3 min to obtain a uniform 50 nm layer. The arrays were patterned on the PMMA layer with a FEI/Philips FIB200 focused ion beam writer, having a liquid Ga^+ ion source operating at 30 kV. The Ga^+ beam is then focused to a 30 nm spot to create the pattern of single-pixel dot arrays on the PMMA; typical beam current is 1 pA and dwell times ($\sim 100\ \mu$s) are varied to change the dot size. The exposed PMMA was then developed in a 1:3 mixture of methyl isobutyl ketone and isopropyl alcohol. The developed samples were coated by a $VO_{1.7}$ layer of 50 nm by pulsed laser ablation (KrF excimer laser at $\sim 4\ \mathrm{mJ/cm^2}$, $\lambda = 248$ nm, and 25 Hz) of a vanadium metal target in a 5 mTorr background O_2 pressure at room temperature. In the lift-off step, the remaining PMMA layer together with its overlayered $VO_{1.7}$ film were removed by a commercial resist remover (Microposit 1165), leaving the $VO_{1.7}$ nanoclusters resting on the Si surface. Finally, oxidation of the NPs was needed to complete their conversion to stoichiometric VO_2. Since vanadium oxide can exist in wide range of stoichiometries, careful control of the oxidation conditions (450 ° C for 20 min in 250 mTorr O_2) is necessary to secure the correct 2:1 oxygen/vanadium ratio in the NPs. The stoichiometry of the pulsed laser deposition grown particles before and

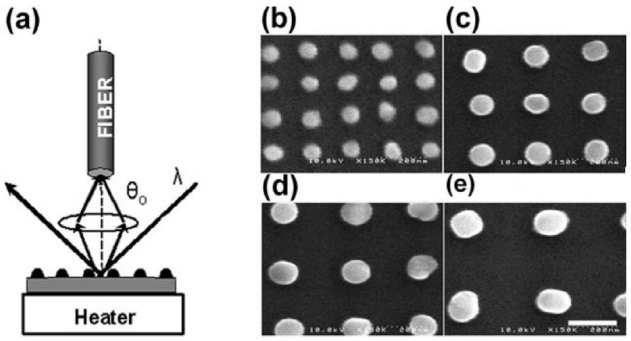

FIG. 1. (a) The dark-field confocal setup used to study the samples. $\theta_o = 60°$. (b) and (c) Scanning electron micrographs of VO_2 arrays with the particle radii $r = 26, 35, 44, 49$ nm and corresponding lattice constant $L = 166, 222, 278, 310$ nm. Scale bar is 200 nm.

after annealing was confirmed by Rutherford backscattering and x-ray diffraction in a separate experiment [12].

Figure 1(b)–1(e) presents micrographs of four of the five used in this experiment. VO_2 does not wet Si and the resulting particles are mostly hemispherical [12]. The particles were arranged in square matrices (60 μm $\times$ 60 μm) with varying periodicities (L) and particle sizes (r), but keeping the ratio L/r constant $\sim$6.3. Keeping L/r constant automatically normalizes the scattering cross section, which is proportional to $(r/L)^2$. More importantly, choosing $L/r > 5$ minimizes near-field particle-particle interactions. It has been shown [5] that for $L/r < 5$, near-field coupling is strong enough to induce shifts in the optical resonances and therefore could potentially obscure our study of the optical size dependence. Thus L/r ratio >5 is a safe regime for our lithography conditions, whereas $L/r \gg 5$ would make the array parameters uncomfortably close to the wavelength of visible light. In that case unwanted ordinary diffractive effects would predominate over the scattering.

We performed dark-field spectroscopy of the NP arrays with a focused nonpolarized white light source as illustrated in Fig. 1(a). The sample is mounted on a Peltier heater and a precision thermocouple is placed near the arrays. The collection objective used to gather the scattered light had a 0.25 numerical aperture (NA) and was operated in confocal mode with a 100 μm multimode optical fiber that delivers the light to an spectrometer with a cooled charge coupled device detector. This dark-field confocal microscopy makes it possible to record spectra from the heart of the NP array with negligible background light. The grating constants of the arrays were kept under 360 nm to avoid diffractive orders collected by the system thus allowing only incoherent scattering [see Eq. (1)].

Figure 2(a) shows the typical spectrum observed of the scattered light from the VO_2 NPs. The blue-green wide peak falls in intensity ($\sim$35%) and blueshifts slightly when the particles switch to the metallic state. This is a unique feature that has not been observed previously in

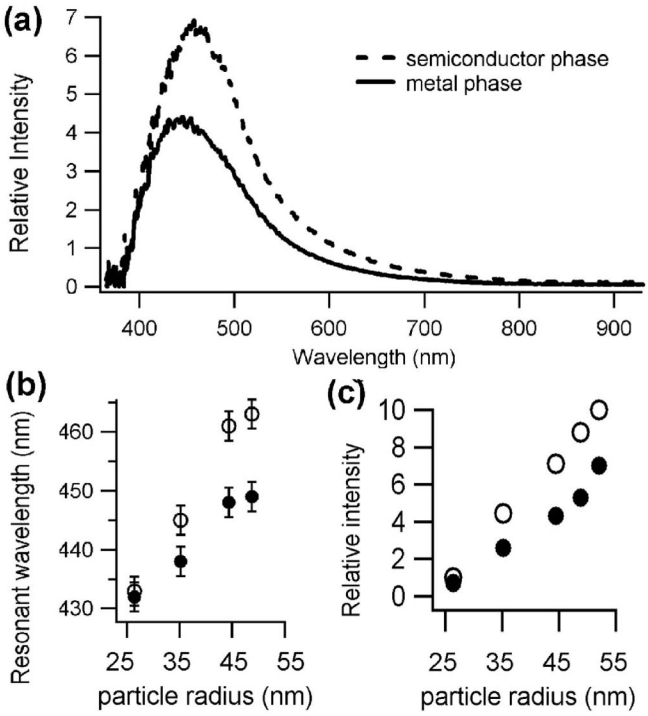

FIG. 2. (a) Scattering spectrum from a VO_2 array ($r =$ 44 nm) at 23 °C and 90 °C normalized to the lamp intensity. (b) Peak position and (c) relative scattered intensity vs particle size in the metallic and semiconducting states (filled and open circles, respectively).

VO_2 bulk samples or thin films, where the largest optical difference between the phases is in the IR. However, we can see that for these NPs, the optical scattering in the IR is quite small. This is because the scattering from small particles presents unique resonances due to the electronic confinement that can be explained in the framework of Mie theory as we show later. Figure 2(b) shows the evolution of this resonance as function of the particle size. There is a pronounced blueshift with smaller sizes, while the shift between the two phases tends to be reduced. The use of these designer arrays allows us to control the intensity of the scattering. With $(r/L)^2$ constant, the scattering intensity is found to be proportional to r as shown in Fig. 2(c).

Another extraordinary behavior is the temperature evolution of the scattered signal at all wavelengths. In VO_2 thin films, one observes narrow, monotonically increasing or decreasing hysteresis curves connecting the two states of the film. In sharp contrast to this behavior, Fig. 3(a) shows that the NP arrays exhibit a broad hysteresis loop with a three-state behavior, the two expected phases plus an additional enhanced intensity state between them. The size effects are not only present in the optical properties but also in the features of the phase transition itself. Figure 3(b) and 3(c) show a correlation between size and phase transition temperatures with higher T_c's for the smaller NPs as well as larger undercoolings and wider hysteresis loops.

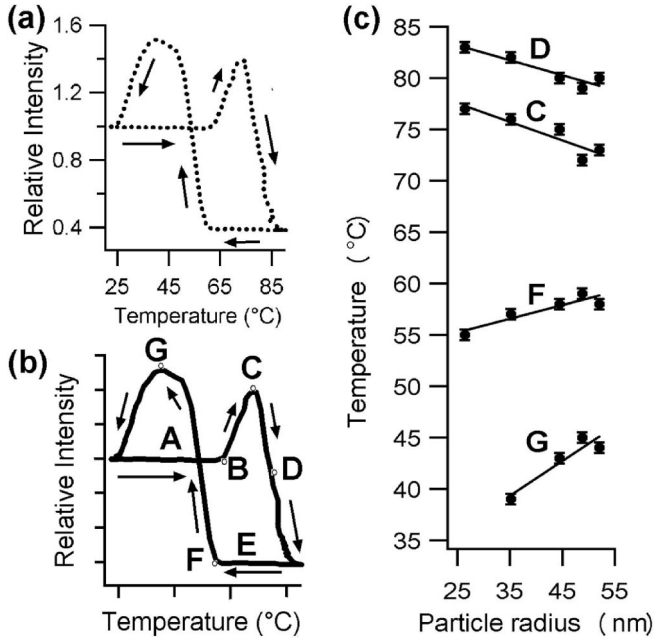

FIG. 3. (a) Temperature evolution of the scattered signal at $\lambda = 600$ nm. (b) Typical hysteresis loop of the scattered light with indicator points along the phase transition from the VO_2 nanoparticles in array. (c) Temperatures of indicator points during a cycle of the VO_2 semiconductor-to-metal phase transition as a function of size. Solid lines are only a guide for the eye.

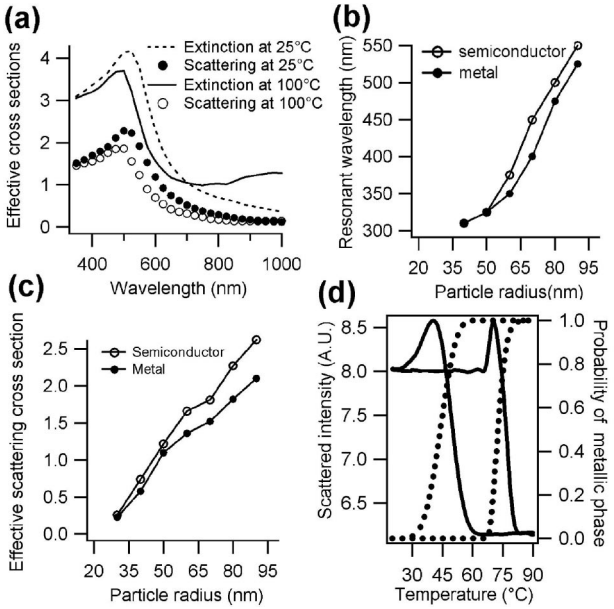

FIG. 4. Calculated optical properties of VO_2 nanoparticles. (a) Mie extinction and scattering effective cross sections for a $r = 80$ nm nanoparticle. (b) Wavelength of resonance vs particle radius. (c) Scattering efficiency vs particle radius. (d) Collective scattered intensity (solid line) for a given probability function (dashed line) of the nanoparticles undergoing phase transition in the array. Notice the less steep cooling side in agreement with observations on Ref. [20].

The extraordinary switching in the visible region is particularly interesting because a resonant response in VO_2 was previously observed only in the infrared due to the surface plasmon of the metallic phase. We can account for the strong size dependence and the visible resonance in the following way. The spatially organized ensemble of VO_2 hemispheres on Si is complicated to model optically from first principles. However, the hemispherical shape and the presence of the Si-air interface has been treated in detail in previous analyses of other NPs, in particular regarding plasmon resonances of metals [13–15]. It has been found that the shape and substrate factors contribute primarily to small redshifts of the spectral features, but do not alter the qualitative features that can easily be modeled using conventional Mie theory. We have performed full Mie calculations [16] using the optical constants [17] of both VO_2 phases. The results shown in Fig. 4(a) present the scattering and total effective extinction cross sections for $r = 80$ nm VO_2 spheres in air. The qualitative agreement with our observation is clear since the scattering cross section presents a peak in the visible region. The contrast between the two phases is evident in the vicinity of that peak but very small in the IR region consistent with our observation. It is important to note that our experiment is mostly blind to absorption effects and the onset of a plasmon resonance at $\lambda = 1$ μm would be only observed in a complete extinction measurement.

Our calculation also predicts the observed blueshift of the resonance with smaller particle size and the lower scattering efficiency for the metallic phase [Fig. 4(b) and 4(c)]. In terms of size comparisons, we observe that the experimental data are redshifted by the presence of the substrate. However, smaller particles will probably quench the effect since the scattering effects are dominant in large particles ($r \geq 50$ nm) whereas absorption dominates for small ones ($r < 10$ nm) [18]. The natural conclusion is that in contrast to the plasmon resonance at $\lambda = 1$ μm that persists in small NPs and is known to have a dipolar source [19], the observed scattering resonance that we have found in the visible is definitely of higher multipolar origin.

Regarding the size dependence of the observed temperatures of the phase transition [Fig. 3(c)], we first point to agreement with previous work [20,21] showing that T_c and the width of the hysteresis loop decreases with increasing particle size. This phenomenon has been explained by the hypothesis that the SMT in VO_2 can be described on the model of a martensitic transformation, in which a density of heterogeneous nucleation centers plays the essential role in triggering the phase transformation [20,22]. For isolated NPs with the same crystallinity, the probability to trigger the structural phase transition at a certain temperature decreases with decreasing NP size as the number of defects within the relevant volume is reduced. Our samples confirm those

previous observations but with the tremendous advantage of controlled average size and narrow size distribution, allowing new insights into the size dependence of the phase transition. We can show that a defined size does not have a unique T_c, but a probability of switching centered at that temperature.

The strict periodicity of the array works as the ideal tool to prove this hypothesis that in earlier studies was clouded by the broad size distribution of particles. Recalling Fig. 3(b), we observe an intermediate intense scattering in the transit region between the two phases. This result arises from the underlying stochastic nature of the phase transition. The VO_2 NPs are arranged in periods L on top of the substrate. When irradiated with light of wavelength λ, the coherent scattered field in the direction θ from each row of NPs will be proportional to:

$$\sum_{n=1}^{N} P_n e^{inL\beta}, \quad \text{with } \beta = \frac{2\pi}{\lambda}(\sin\theta_0 - \sin\theta). \qquad (1)$$

P_n is the scattering efficiency of the nanoparticle n. Clearly when β is a multiple of $2\pi/L$, the scattering would be coherent. For $L < \lambda$ and large N the sum tends to cancel by destructive interference at the collection angle $\sin\theta \leq \mathrm{NA}$, resulting in a low intensity, characteristic of the P_n scattering efficiency of the nanoparticles. This efficiency was shown above to be greater for particles in the semiconducting state than in the metallic one, $P_n^{\text{semiconductor}} > P_n^{\text{metal}}$. However, when the particles start to transform, the incoherent scattering fails to minimize the sum in Eq. (1) since the lowest Fourier frequency needed to describe the array becomes smaller than $2\pi/L$. This explanation is modeled in Fig. 4(d) for a linear chain of 100 particles switching with a probability function that transforms particles of the chain with a random number generator. At the point of maximum disorder of the chain, the scattering peaks, in a clear order-disorder-order transformation that the array follows in transforming into the other phase. For all samples, the onset of the phase rising is at bulk T_c [point B in Fig. 3(b)], but the peak shifts [point C in Fig. 3(b)] with particle size in evidence of the stochastic nature governing the actual size dependence.

In summary, the optical contrast between the semiconducting and metallic phases of VO_2 NPs in ordered arrays is dramatically enhanced in the visible region, exhibiting size-dependent multipole optical resonance and transition temperatures. The collective optical response shows an enhanced scattering state as the phase transition progresses, due to the intrinsic variability in the transition temperature of the individual elements of the optical array. These new observations provide critical insights into statistical processes occurring in materials at the nanoscale. These properties also constitute an important set of size-dependent features that become more and more relevant as VO_2 approaches nanotechnology applications [23,24].

This material is based upon work supported by the National Science Foundation under Grant No. DMR-0210785. The authors acknowledge useful technical discussions with A. B. Hmelo.

*Electronic address: rene.lopez@vanderbilt.edu
†Also at The Condensed Matter Division, Oak Ridge National Laboratory, Oak Ridge, TN 37831, USA.

[1] J. D. Joannopoulos, P. R. Villenueve, and S. Fan, Nature (London) **386**, 143 (1997).
[2] A. J. Haes and R. P. V. Duyne, J. Am. Chem. Soc. **124**, 10 596 (2002).
[3] S. A. Maier, P. G. Kik, H. A. Atwater, S. Meltzer, E. Harel, B. E. Koel, and A. A. G. Requicha, Nat. Mater. **2**, 229 (2003).
[4] N. Félidj, G. L. J. Aubard, J. R. Krenn, G. Shider, A. Leitner, and F. R. Aussenegg, Phys. Rev. B **65**, 075419 (2002).
[5] L. Zhao, K. L. Kelly, and G. C. Schatz, J. Phys. Chem. B **107**, 7343 (2003).
[6] H. R. Stuart and D. G. Hall, Phys. Rev. Lett. **80**, 5663 (1998).
[7] S. Linden, J. Kuhl, and H. Giessen, Phys. Rev. Lett. **86**, 4688 (2001).
[8] J. B. Goodenough, J. Solid State Chem. **3**, 490 (1971).
[9] R. M. Wentzcovitch, W. W. Schulz, and P. B. Allen, Phys. Rev. Lett. **72**, 3389 (1994).
[10] A. Zylbersztejn and N. F. Mott, Phys. Rev. B **11**, 4383 (1975).
[11] A. Cavalleri, C. Tóth, C. W. Siders, J. A. Squier, F. Raksi, P. Forget, and J. C. Kieffer, Phys. Rev. Lett. **87**, 237401 (2001).
[12] J. Y. Suh, R. Lopez, L. C. Feldman, and R. F. Haglund Jr., J. Appl. Phys. **96**, 1209 (2004).
[13] R. Chauvaux and A. Meessen, Thin Solid Films **62**, 125 (1979).
[14] J. L. Bijeon, P. Royer, J. P. Goudonnet, R. J. Warmack, and K. L. Ferrett, Thin Solid Films **155**, L1 (1987).
[15] G. Videen, J. Opt. Soc. Am. A **8**, 483 (1991).
[16] H. C. van de Hulst, *Light Scattering by Small Particles* (Dover, NY, 1981).
[17] H. W. Verleur, A. S. Baker, and C. N. Berglund, Phys. Rev. **172**, 788 (1968).
[18] I. O. Sosa, C. Noguez, and R. G. Barrera, J. Phys. Chem. B **107**, 6269 (2003).
[19] R. Lopez, T. E. Haynes, L. A. Boatner, L. C. Feldman, and R F. Haglund Jr., Opt. Lett. **27**, 1327 (2002).
[20] R. Lopez, T. E. Haynes, L. A. Boatner, L. C. Feldman, and R. F. Haglund Jr., Phys. Rev. B **65**, 224113 (2002).
[21] V. A. Klimov, I. O. Timofeeva, S. D. Khanin, E. B. Shadrin, A. V. Ilinskii, and F. Silva-Andrade, Technical Physics **47**, 1134 (2002).
[22] I. A. Kharhaev, F. A. Chudnovskii, and E. B. Shadrin, Phys. Solid State **36**, 898 (1994).
[23] A. A. Bugayev and M. C. Gupta, Opt. Lett. **28**, 1463 (2003).
[24] S. Chen, H. Ma, X. Yi, H. Wang, X. Tao, M. Chen, X. Li, and C. Ke, Infrared Phys. **45**, 239 (2004).